RECENT CHANGES IN THE MCMURDO ICE SHELF TRANSITION ZONE AND HUT POINT PENINSULA, WEST ANTARCTICA

Ann M. Hill[1,2], Kristin M. Schild[1,2], Seth W. Campbell[1,2,3], Sarah F. Child[4]

[1] University of Maine, School of Earth and Climate Sciences; Orono, ME, USA

[2] University of Maine, Climate Change Institute; Orono, ME, USA

[3] U.S. Army Cold Regions Research and Engineering Laboratory (CRREL); Hanover, NH, USA

[4] Cooperative Institute for Research in Environmental Sciences (CIRES), University of Colorado; Boulder, CO, USA

Corresponding Author: Ann M. Hill; hillann1010@gmail.com

ABSTRACT

McMurdo Ice Shelf (MIS) and Ross Island act as both lateral margins and pinning points for the Ross Ice Shelf, as well as logistic hubs for the United States and New Zealand Antarctic Programs. Recent thinning and retreat of MIS has motivated an evaluation of the future stability of this critical region and potential adaptation. If MIS were to collapse, it could initiate sizeable teleconnections across West Antarctica, as well as stifle Antarctic research that relies on MIS/Ross Island-based logistics. One logistics component already experiencing change is the transition zone (TZ) road, which connects MIS with the research stations on Hut Point Peninsula (HPP), Ross Island. Here we assess the vulnerability of the TZ road and a proposed rerouting location (TZ Hillside), by using a combination of *in situ*, remote sensing, and numerical modeling approaches. We evaluate overall elevation change by differencing late summer, WorldView-derived, DEMs (2011–2015), and evaluate the practicality of both a stable ice surface and bare earth road using a numerical ice volume flux model, informed by GPR and GPS measurements of ice thickness and velocity (2015–2016). Results show overall ice elevation change of up to 3 m, and 204 ± 24 m^3 a^{-1} of ice flux across the TZ Hillside. Combined, these

results indicate that the TZ Hillside is unsuitable for either type of road, and point to MIS terminus retreat and TZ Hillside melt as a continuing risk for TZ stability, which could prelude broader changes.

KEYWORDS: Ice Shelf, Remote Sensing, Antarctica, McMurdo, Elevation Change

1. INTRODUCTION

Ice shelves surround over 75% of the Antarctic coastline (e.g., Rignot et al., 2013) and provide critical stability to the Ice Sheet primarily through tributary glacier buttressing. Due to their flat, thick nature, ice shelves can also be a pivotal logistic resource, serving as a runway for large aircrafts (e.g., Haehnel et al., 2019), a road for overland traverses (e.g., Lever & Thur, 2014), and a staging location for scientific operations (e.g., Millan et al., 2013). The McMurdo Ice Shelf (MIS) is one such location that is critical for both glacier stability and field logistics. The MIS buttresses Skelton, Terror, Aurora, and Koettlitz Glaciers (Fig. 1) and also acts as a lateral shear margin to the adjacent Ross Ice Shelf (RIS), which drains both East (EAIS) and West Antarctic Ice Sheets (WAIS). The thinning, retreat, or collapse of MIS could trigger a retreat of RIS, inducing thinning and potential acceleration of ice streams over 900 km away (e.g., MacAyeal and Bindschadler Ice Streams; Reese et al., 2018). Additionally, increased meltwater flux and ponding has the potential to facilitate destabilizion of MIS near its terminus (e.g., Scambos et al., 2000), particularly if the ponding is not drained (Banwell et al., 2013; Banwell et al., 2019). MIS also serves as the primary logistics hub for the United States (McMurdo Station) and New Zealand (Scott Base) Antarctic Programs. Therefore, due to the

prominent role of MIS in both ice sheet stability and Antarctic infrastructure, understanding the stability of MIS is critically important.

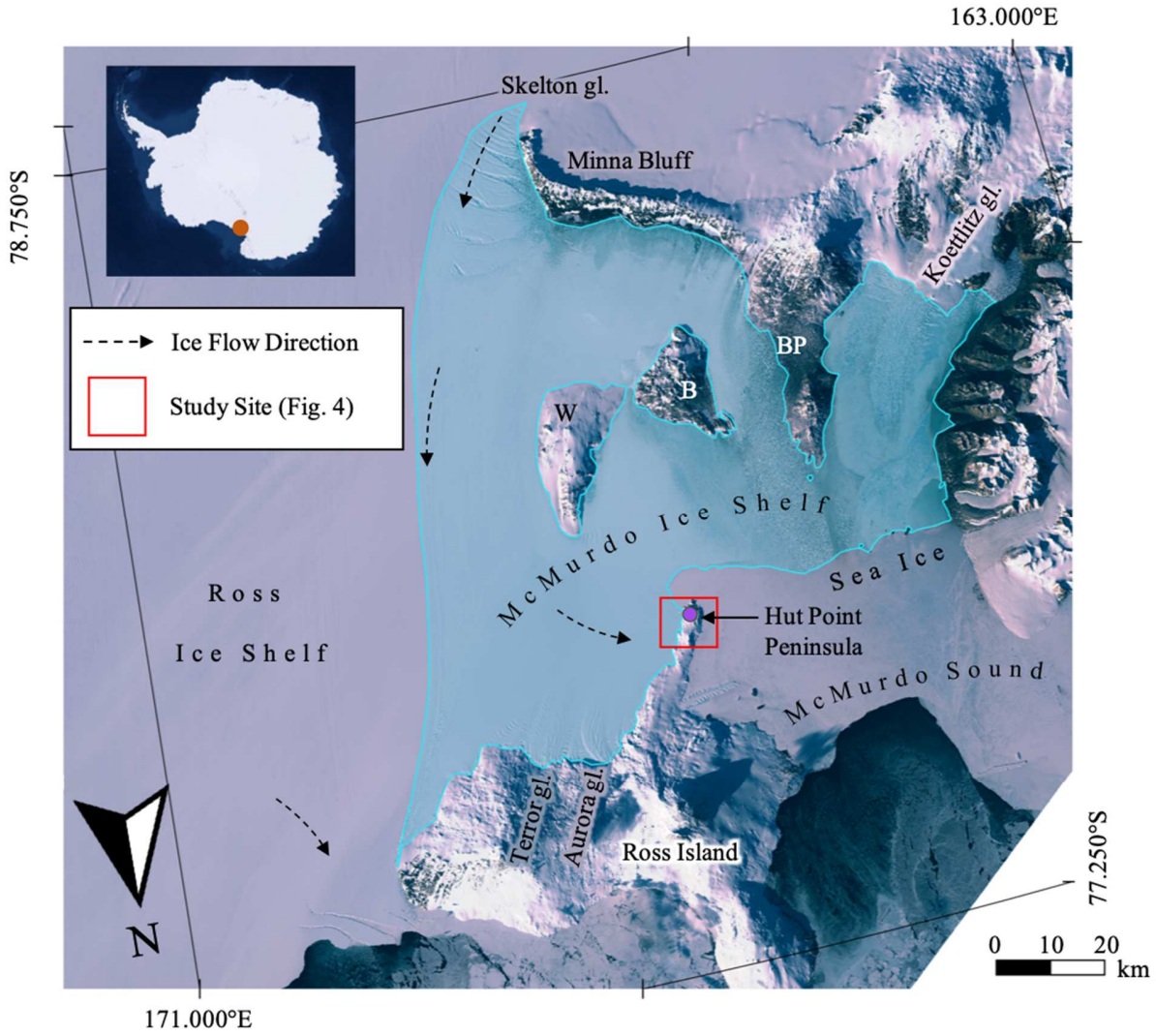

Figure 1. The McMurdo Ice Shelf (MIS) and Hut Point Peninsula (HPP) study region (inset, orange circle), where MIS (turquoise shading) is bound by the Ross Ice Shelf, and McMurdo Sound. Noted are the locations of the NOAA AWS (purple circle), White Island (W), Black Island (B) and Brown Peninsula (BP). Ice flow directions are denoted by dashed arrows (established in Campbell et al., 2017) with tributary glaciers (gl.) labeled. Background true color image is from Sentinel-2, collected on 11 October 2019.

The stability of an ice shelf is directly related to its mass balance and resistance to flow at its lateral margins. Ice shelf mass balance is controlled through surface accumulation or ablation (including calving), tributary glacier flux, and basal freeze-on or melt. Lateral ice shelf margins resist ice flow either by friction against bedrock or via slower moving lateral ice (e.g., MacGregor et al., 2012). Therefore, thinning or collapse of an ice shelf at its margins decreases or removes a primary resistance to ice flow. Additionally, ice shelves also provide a buttressing force to tributary glacier flow, therefore any reduction in ice shelf mass, results in a decrease in buttressing force, and can enable tributary glacier speedup and dynamic thinning (e.g., Scambos et al., 2004; Hulbe et al., 2008). Lastly, while tributary glaciers act to increase ice shelf mass, the glaciers themselves are also responding to their own mass balance. Therefore, a decrease in tributary glacier mass balance will ultimately translate down-glacier to ice shelves via reduced ice volume influx. Currently, most ice shelves in Antarctica are losing more mass than they are gaining, primarily through a complex combination of calving icebergs, surface melting, and basal melting (e.g., Depoorter et al., 2013; Rignot et al., 2013; Bell et al., 2017; Kingslake et al., 2017; Smith et al., 2020).

The thickness of an ice shelf also contributes to its stability. Antarctic ice shelves can range in thickness from 2000 m at the grounding line to 100 m at the ice shelf terminus; however, MIS is thinner than most, ranging between ~6–200 m thick (Glasser et al., 2006; Campbell et al., 2017). In the Ross Island region, RIS and MIS are particularly susceptible to basal melting due to the routing of warm Antarctic Surface Water (ASW) directly under this region (Rack et al., 2013; Stern et al., 2013; Tinto et al., 2019). While recent models (Tinto et al., 2019) and field geophysical observations (Stewart et al., 2019) are not completely aligned in

79 establishing the exact melt rate, both studies suggest higher basal melt rates closer to White and
80 Black Islands as opposed to Hut Point Peninsula (HPP). This region of MIS, near White and
81 Black Islands, also experiences unusually high surface melt ranging from 43–441 mm w.e.
82 during a summer melt season, resulting in approximately 25% of the region around Black Island
83 becoming flooded with streams and ponds during this time (Glasser et al., 2006). Adding to the
84 spatial complexity, a winter accumulation gradient can also be inferred from geophysical
85 observations across MIS suggesting higher rates of accumulation near HPP and lower rates of
86 accumulation near White and Black Islands (Campbell et al., 2017). Despite higher rates of
87 accumulation near HPP, surface mass balance of Ross Island, which contributes to the mass
88 balance of MIS via ice influx, is relatively unknown. Concerningly, the combination of a
89 thinning MIS from surface and basal melt or reduced ice flux, and the abundance of surface
90 water present (Banwell et al., 2013; Banwell et al., 2019), may not require much tidal flexure to
91 bypass a rapid disintegration threshold. As atmospheric and oceanic temperatures continue to
92 warm, continued evaluation of contributions to MIS stability are essential for both scientific and
93 logistic concerns.

94 Stemming from the importance of MIS in Antarctic logistics, several "single-point
95 failures" in the MIS-HPP system have been identified that would jeopardize the feasibility of
96 using MIS and HPP for United States and New Zealand Antarctic logistics (Augustine et al.,
97 2012). One such failure would be reduced access between HPP, where Scott Base and McMurdo
98 Station are located, and MIS, where all runway and aircraft operations are located. Currently, the
99 primary road connecting MIS to HPP is by the Pegasus Ice Road, which crosses the Transition
100 Zone (TZ) (Fig. 2). The TZ is a triaxial point of stress where MIS buttresses against HPP at the
101 ice shelf–sea ice transition. This buttressing of ice leads to compression folds, severe fracturing,

and complex ice dynamics (Campbell et al., 2017; Fig. 2). Meltwater runoff from the nearby Hillside of HPP has caused severe ponding in the TZ. While the ponding is partially alleviated by drain holes into the relatively porous fractured ice shelf (Shoop et al., 2014), the englacial influence of meltwater at the TZ, and complex dynamics in this area, are concerning for long-term stability and longevity of Pegasus Ice Road. In this study we assess the feasibility of a new road location that would circumvent this TZ single-point failure location.

This study focuses on the yet-to-be characterized surface mass balance of HPP and the location of the MIS terminus, addressing both science and logistical concerns. We analyze recent changes in ice elevation across the TZ and surrounding region and explore a proposed new road location on the TZ Hillside, which would connect MIS with HPP and replace Pegasus Ice Road in the event the current route becomes unpassable (Fig. 2, white line). To determine if there is any evidence of MIS-HPP instability, we corrected and differenced satellite-derived digital elevation models (DEMs) acquired several years apart to spatially measure elevation changes (inferring ice thickness changes) across HPP and MIS. To explore the proposed new road location on the TZ Hillside, we completed ground-penetrating radar (GPR) and GPS surveys to measure ice thicknesses and ice flow velocities, respectively. We then used three-dimensional finite element numerical modeling to calculate ice flow flux on the TZ Hillside and estimate potential ice flow impacts to the proposed new road location.

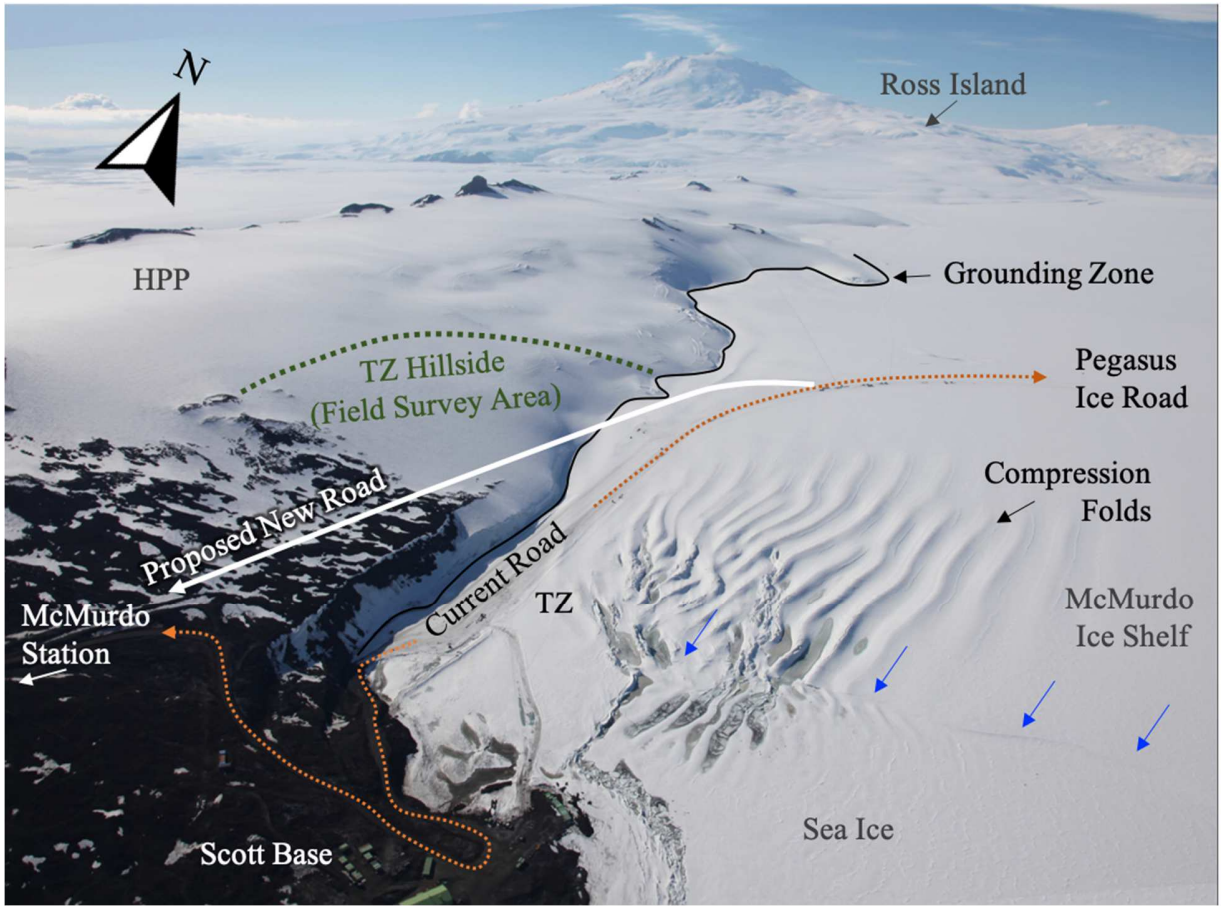

Figure 2. Airborne image of Hut Point Peninsula (HPP), on Ross Island. Noted are the locations of the transition zone (TZ), the McMurdo Ice Shelf (MIS) terminus (blue arrows), the grounding zone (black solid line), the Pegasus Ice Road (orange dotted line), which is the current road from MIS onto HPP, the proposed new road between MIS and HPP (white solid line), and the GPR and GPS field survey area on the TZ Hillside (green dotted area).

2. METHODS

2.1. Surface Elevation Change

To quantify elevation changes across the HPP-MIS region, we established a new workflow (schematically depicted in Fig. 3) combining *in situ* data, remote sensing

measurements, and numerical modeling results to accurately co-register DEM pairs prior to differencing. In addition to minimizing the impact of terrain shadows and clouds on vertical measurements, we also isolated variability in the TZ region due solely to changes in tidal phase and amplitude, and atmospheric pressure (e.g., Kulshrestha et al., 2020). This workflow and relevant data sets are more thoroughly described in the following sections (sections 2.1.1. – 2.1.4.).

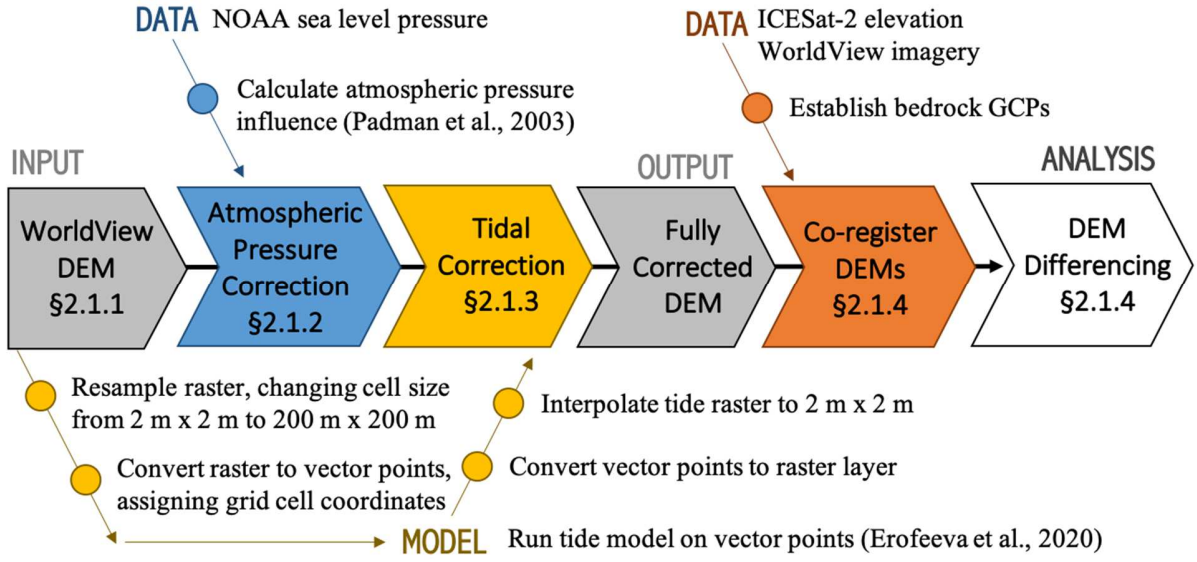

Figure 3. Schematic diagram outlining the steps and data sets used in the developed method to correct each DEM prior to differencing. This method accounts for differences in atmospheric pressure (blue) and tidal amplitude (yellow) between DEMs, as well as variability in DEM processing (orange).

2.1.1. DEM generation and filtering

To quantify the change in ice elevation across HPP and MIS, we estimated the hypsometric variation of the grounded glacial ice and surrounding ice shelf (Fig. 1, red box)

using Reference Elevation Model of Antarctica (REMA) 2 m resolution DEM strips (Howat et al., 2019). These elevations are generated from Maxar's WorldView imagery using the Surface Extraction with TIN-based Search-space Minimization (SETSM) algorithm (Noh & Howat, 2015) to calculate stereo-parallax with each image's rational polynomial coefficients. Potential errors in SETSM processed DEMs arise from extreme shadowing effects, clouds, and image acquisition from various off-nadir degrees (Child et al., 2020). To account for these errors, we removed spurious elevations via manual inspection of DEM hillshade maps and unprocessed WorldView imagery. Due to variability in DEM spatial coverage, elevation change between 2011 and 2015 was calculated using different DEM pairs for grounded ice and the ice shelf to maximize the extent of the results, therefore DEMs from 6 February 2011, 14 March 2011, and 16 February 2015 were prepared for differencing.

2.1.2. Atmospheric Pressure Correction

The elevation of a freely floating ice shelf is impacted by changes in atmospheric pressure; therefore, differences in atmospheric pressure between data collection days could result in erroneous measurements of vertical change. To remove the impact of atmospheric pressure, we used the ice shelf correction established in Padman et al. (2003), where a pressure difference of 1 hPa between the measured value and standard atmospheric pressure (1013.25 hPa) results in 0.82 cm adjustment in elevation. To determine atmospheric pressure, we used the National Oceanic and Atmospheric Administration (NOAA) National Centers for Environmental Information site (https://www.ncei.noaa.gov/products), located adjacent to McMurdo Station (Fig. 1, purple circle), at the closest measurement in time (25-28 min) to the image acquisition

168 time. We then adjusted the ice shelf (Fig. 1, teal shaded region) in each DEM to standard
169 atmospheric pressure.
170
171 *2.1.3. Tidal correction*
172 Ice shelf elevation is also impacted by the tidal signal; without correction, differences in
173 tidal phase and amplitude between the DEM pairs would result in erroneous measurements of ice
174 shelf elevation change. The tidal signal was calculated using the Tidal Model Driver (TMD;
175 Padman & Erofeeva, 2005) 2.5 (Erofeeva et al., 2020). Due to the small degree of spatial
176 variability in the tidal signal (0.1–0.3 m over 11.32 km^2), we ran the tidal height model at a
177 down-sampled (200 m) spatial resolution to expedite processing; the tidal height results were
178 then interpolated to the original 2 m DEM spatial resolution before being applied to the ice shelf
179 portion of each DEM.
180
181 *2.1.4. DEM Differencing*
182 To minimize the impact of seasonal variability on interannual elevation changes, we
183 focused on using only DEMs collected at the end of the austral summer season; however,
184 nonuniformities in the spatial extent of each DEM necessitated that elevation change between
185 2011 and 2015 be calculated using slightly different austral summer DEM pairs for grounded ice
186 (14 March 2011 and 16 February 2015) and the ice shelf (6 February 2011 and 16 February
187 2015). After removing erroneous data due to off-nadir data collection, shadows, and clouds, and
188 correcting for the tidal signal and atmospheric pressure in each DEM, we co-registered the DEM
189 pairs to correct for transformation shifts (Paul et al., 2015; Paul et al., 2017) caused by terrain
190 slope and aspect and varying image acquisition parameters (section 2.1.1.). To co-register the

DEM pairs we used stable terrain points — non-ice, exposed bedrock with slopes < 20°— from REMA (n=84,814 points; following the methods of Nuth & Kääb, 2011 using code from McNabb, 2019). We compared the corrected, co-registered DEMs with ground control points (GCPs) constructed from overlapping stable terrain and ICESat-2 tracks (n=6-7 points) to validate the absolute elevation (average offset of 1.28 m). After taking the difference of the co-registered DEMs, we quantified the error over stable terrain by calculating a second-degree polynomial surface and removed from the full differencing results (Racoviteanu et al., 2007). The range in the trend was -2.8 to 3.4 m and the removal resulted in a very strong relative agreement between DEM pairs of 0.008 m ±1.89 m.

2.2. Subsurface Ice Structure

To measure the subsurface structure of Pegasus Ice Road and evaluate the possibility of relocating the road to the TZ Hillside, we performed GPR surveys in both of these regions. We collected three 840 m parallel GPR transects (2.5 km total), spaced ~10 m apart, on Pegasus Ice Road in January 2016 using a 400MHz antenna, as well as four parallel and one cross-cutting transect on the TZ Hillside in November 2016 (5.5 km of 100 MHz and 4.7 km of 400 MHz). To perform these GPR surveys, we used a Geophysical Survey System Incorporated (GSSI) SIR-4000 control unit coupled with a GSSI model 3207AP 100 MHz antenna and GSSI model 50400 400 MHz antenna. We recorded scans for 1000–1400 ns, with a two-way travel time (TWTT) at 24 scans s^{-1}, and 2048 samples per scan. High and low pass finite impulse response filters were used during data collection; between 100–800 MHz for the 400 MHz antenna and between 25–300 MHz for the 100 MHz antenna. The GPR was synced with a handheld Garmin GPSMap78, recording GPS position at 1 Hz. The GPR antennas were hand-towed at approximately 0.25 m s^{-}

[1] resulting in traces approximately every 1 cm and GPS positions every 0.25 m. Estimated horizontal precision of GPR profiles from the handheld GPS was ±2 m.

To convert TWTT to depth, we first calculated the velocity of the radio waves through the substrate, using the equation $V = \frac{c}{\sqrt{\dot{\varepsilon}}}$, where $\dot{\varepsilon}$ is relative permittivity, V is the radio wave velocity in m ns^{-1}, and c is the speed of light in m s^{-1}. For depth calibration of the Pegasus Ice Road and the TZ Hillside, we used different values for permittivity ($\dot{\varepsilon}$) as the surface types varied from snow and firn (Pegasus Ice Road) to solid ice (TZ Hillside). For the Pegasus Ice Road transects, we used a relative permittivity value of 2.8, based on depth-density results from a shallow core collected within the TZ region (Campbell et al., 2017), which shows that dense firn ($\dot{\varepsilon}$~ 2.2) is overlying meteoric and marine ice ($\dot{\varepsilon}$~3.1). For the TZ Hillside, we used the relative permittivity of ice ($\dot{\varepsilon}$ = 3.1) for depth calculations, as the TZ Hillside was primarily composed of bare ice with only 20–50 cm of snow cover. Based on the TWTT and calculated wave velocity (0.169–0.179 m ns^{-1}), we recorded ~60 samples per m depth, which is more than sufficient for a smooth waveform given the frequencies used. The GPR profiles were processed using GSSI commercial software (RADAN v. 7.0), and processing included time-zero correction, horizontal filtering to remove ringing, and stacking to improve signal-to-noise ratios and visualization of englacial structure.

2.3. TZ Hillside Ice Velocity

2.3.1. In situ surveys

To calculate regional ice velocity and rates of deformation at the proposed road site, we placed 22 bamboo stakes (2 m in length) in a grid configuration on the TZ Hillside and performed kinematic GPS surveys at these locations. Stakes were installed by hand drilling 1 m

236 holes using a Kovacs auger. Kinematic GPS surveys were conducted using a roving Trimble
237 NetR7 and Zephyr Geodetic Antenna unit, with an identical geodetic GPS base station
238 established at McMurdo Station (2–2.6 km from survey grid). We first surveyed the stakes on
239 12–15 November 2015 and then resurveyed the stakes on 2 January 2016 (47–51 days between
240 surveys). Using changes in position, we estimated ice flow velocities and rates of deformation
241 for this TZ Hillside region. Systematic position uncertainty from the processed baselines was 1.9
242 ± 0.01 cm in the horizontal and 4.7 ± 1.9 cm in the vertical. We also assumed 1 cm of bias
243 uncertainty due to the stake hole size relative to the distance measured and leveling of the survey
244 rod. Combining systematic and bias uncertainty, our total horizontal positional error is 2.1 cm at
245 each measurement.
246
247 *2.3.2. Numerical Modeling*
248 To better resolve the rates of deformation on the TZ Hillside, and determine the
249 suitability of this region for the proposed new road, *in situ* GPS and GPR measurements were
250 used to constrain a three-dimensional numerical model. We used surface elevation and ice
251 thickness measurements from the GPS and GPR surveys, respectively, to develop raster layers,
252 which we merged to constrain top and bottom surfaces of a finite element numerical model in
253 COMSOL Multiphysics (v. 5.2a). Model boundary conditions included a no-slip (frozen) bed,
254 normal surface stress, and open boundaries at the inlet (top of the hillside) and outlet (bottom of
255 the hillside near the grounding zone). Open boundaries are standard within COMSOL to
256 represent a geometric boundary separating the modeled domain from non-modeled domain.
257 Despite the geometric boundary, an "open" boundary indicates that material can enter or exit the
258 modeled domain via the geometric boundary, following the prescribed physics of the material (in

this case, ice). We set the model to have minimal snow and/or firn cover, which allowed for a constant density (ρ) of ice, and used a cold-ice viscosity (μ) of ~1×10^{15}Pa s (Marshall, 2005). Given the prescribed boundary conditions and rheology, ice flow was driven by gravitational forcing and internal ice deformation. Model results of surface velocity were compared to stake-derived surface velocities to analyze model accuracy and robustness; we found the model velocity to be comparable to the measured velocity within ±0.1 m a^{-1}. The model was then used to estimate ice volume flux across the TZ Hillside along the proposed new road location. Despite HPP being situated immediately above the grounding zone of MIS, likely causing a complex basal boundary condition down-glacier from the proposed road, our close agreement between GPS-measured velocities and modeled velocities on the TZ Hillside suggest that our model provides a reasonable approximation of ice volume flux.

3. RESULTS

3.1. Spatial variability of HPP region

After correcting and differencing the 2011 and 2015 DEMs, we found a retreat of the ice shelf terminus, and predominantly negative elevation changes across the MIS-HPP region. The elevation change on MIS ranges from -2.8 to 1.9 m (mean: -0.34 m ± 0.77 m) across this 4-year time span, with focused gains adjacent to the newly retreated terminus and losses upstream. These results are consistent with prior results showing a net thinning of the ice shelf as well as the impact of terminus retreat on near-terminus flotation (Hogg et al., 2021). As the ice shelf DEMs were not corrected for ice movement, some features across MIS, namely the compression folds and Pegasus Ice Road, highlight these dynamic changes in their elevation change. The compression folds show both increasing and decreasing elevation change, highlighting the

troughs and peaks of the surface topography and indicating a migration of the folds. The Pegasus Ice Road appears in two locations, and indicates a migration of the road due solely to ice shelf flow. The variable distance in spacing between the two locations (overlapping at the TZ with increasing separation with distance on MIS). Is consistent with variable ice shelf velocities during this 4-year period (Fahnestock et al., 2016; Scambos et al., 2019). In the north-central region of HPP, the elevation slightly decreased, while the northeast slope experienced the largest elevation decreases, resulting in an average change of -0.34 ± 0.77 m (range: -1.99 to 2.00 m) across HPP. This overall net loss across HPP and MIS aligns with previous findings using different methods (Campbell et al., 2018) suggesting that this study robustly captures surface elevation changes.

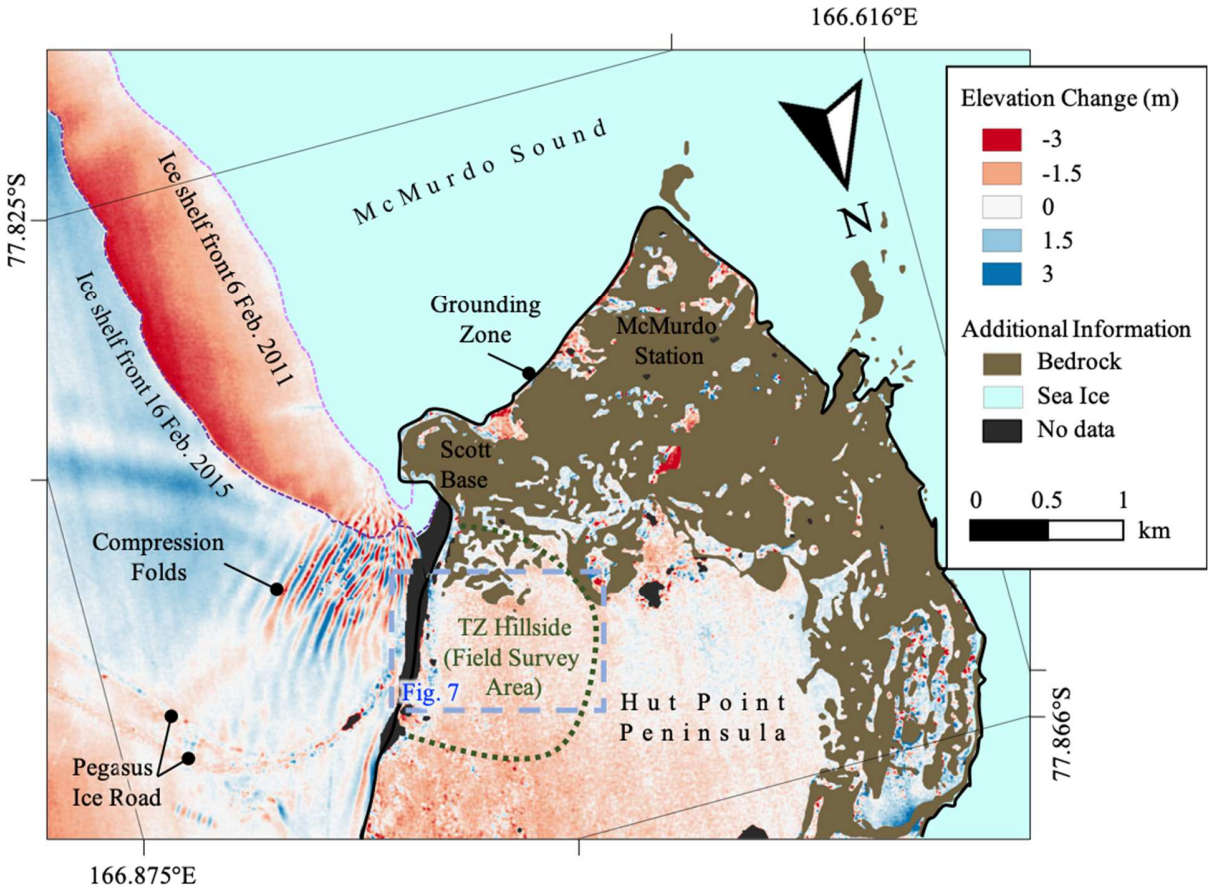

Figure 4. Surface elevation change on McMurdo Ice Shelf (MIS) between 6 February 2011 and 16 February 2015, and on Hut Point Peninsula (HPP) between 4 March 2011 and 16 February 2015. The corrected DEM differencing for this study site (Fig. 1, red box) shows ice shelf terminus retreat (light and dark purple dashed lines, across HPP. DEM differencing also highlights ice shelf movement between scenes, with a migration of both the compression folds and Pegasus Ice Road.

3.2. Ice Structure

3.2.1. Pegasus Ice Road Structure

The GPR profiles collected on the Pegasus Ice Road (Fig. 5) reveal structure to ~20 m depth and surface conformable stratigraphy (SCS) in the top 3–5 m. Thicker conformable stratigraphy is visible within syncline folds (SF) crossing the road. Below the SCS, heavily deformed, discontinuous, and dipping horizons are present. At 12–15 m depth, a series of stratified and discontinuous layers are prevalent. The near-surface stratigraphy is likely recent accumulation and firn reworked during yearly road construction over heavily deformed and fractured ice, while the strong GPR horizons at 12–15 m depth likely represents discontinuous marine ice frozen onto the bottom of meteoric ice (e.g., Campbell et al., 2017). Vertical noise bands originate from specific horizons near 5 m depth, which we interpret to be caused by laterally continuous water tables within the firn. These horizons occur near the base of the SCS, which supports our interpretation that the conformable stratigraphy is composed of permeable firn and the discontinuous layers below are likely impermeable meteoric glacier ice. This geophysical response to water in glacier snow or firn is a well-documented phenomenon (e.g., Campbell et al., 2012; Forster et al., 2014).

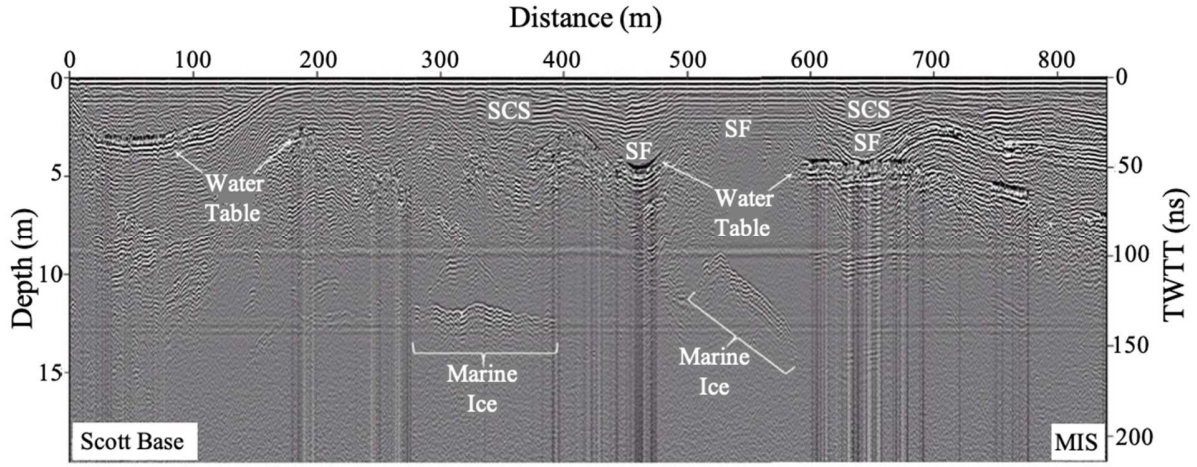

Figure 5. A 400 MHz GPR profile collected along the Pegasus Ice Road in January 2015 Profile shows near-surface conformable stratigraphy (SCS), complex syncline folds (SF), discontinuous stratified marine ice below, and vertical noise bands, which we interpret to be caused by water resting on the firn–ice transition. This GPR transect is displayed from Scott Base on left to MIS on right (GPR profile location is shown in Fig. 7).

3.2.2. TZ Hillside Ice Structure

The 400 MHz and 100 MHz antennas were both used to survey the TZ Hillside and quantify subsurface stratigraphy. Both antennas successfully imaged bedrock to ~65 m depth on the TZ Hillside, with greater thicknesses near the top of the hill and shallower depths located near the bottom, just above Pegasus Ice Road (~40–50 m thick). Profiles collected along the proposed new road on the TZ Hillside show relatively flat subglacial topography and ice thicknesses reaching 40 m depth. At the top of the hill, a buried symmetrical bedrock feature rises to within 25 m of the surface (Fig. 6). Substantial noise, high attenuation rates, and limited or no stratigraphy occurs within the radar data above the bedrock rise. Similar complex stratigraphy and noise has been observed in GPR profiles from temperate glaciers where snow,

firn, or ice has been thermally altered thereby destroying stratigraphic horizons via chemical diffusion (Campbell et al., 2012). Elsewhere across the TZ Hillside, conformable stratigraphy is visible to 20–25 m depth in both the 400 MHz (Fig. 6a) and 100 MHz (Fig. 6b) data.

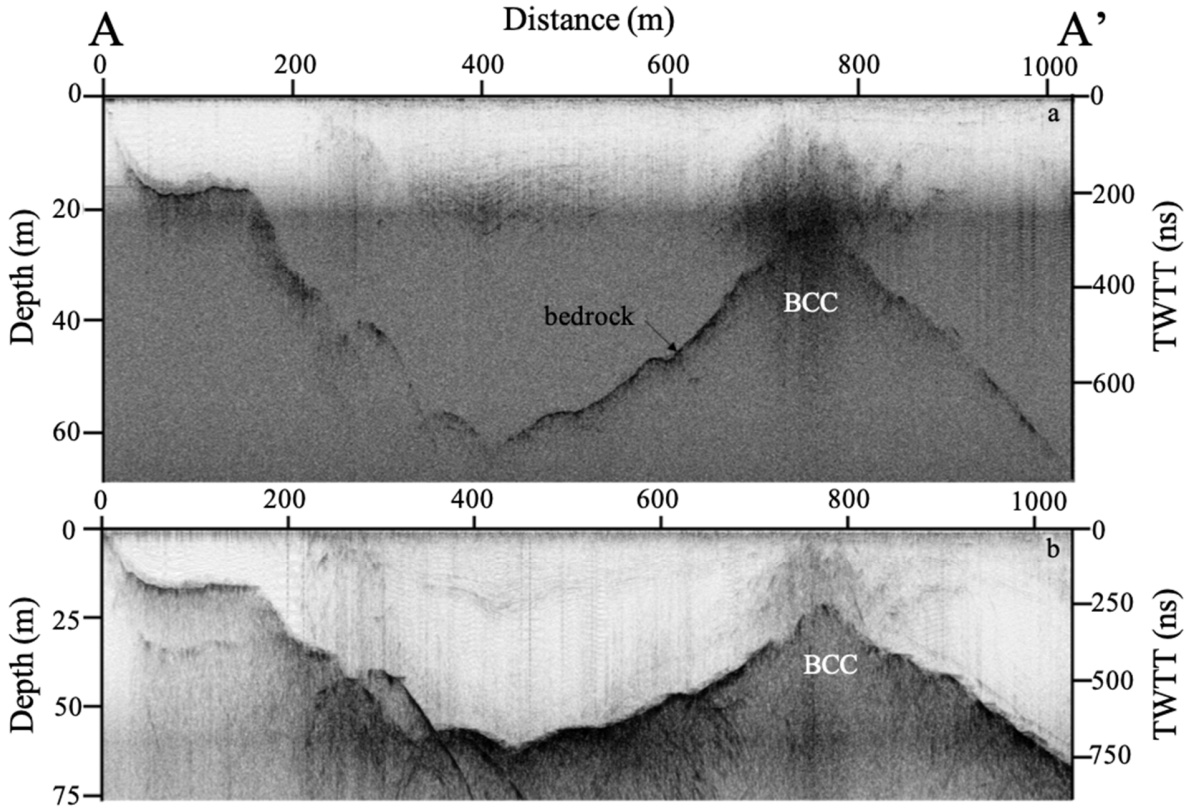

Figure 6. One of the parallel GPR transects on the TZ Hillside (location noted in Fig. 7), showing the 400 MHz profile (a) and 100 MHz profile (b) with the bedrock topography and potentially buried cinder cone (BCC) noted. The complex stratigraphy above the cone is similar to noise imaged by GPR within temperate glaciers, suggesting that the ice has been thermally altered above the cone. Therefore, we suggest that ice has been situated overtop of the cone since its initial formation, or at a minimum, since recent thermal activity.

3.3. Ice Velocity Profiles

344 *3.3.1. In situ surveys*

345 Repeat kinematic GPS surveys of the 22 bamboo poles installed on the TZ Hillside
346 revealed average ice-flow velocities from 0.1–1.1 ± 0.167 m a^{-1} with the highest velocities
347 located in the eastern corner of the grid and near the bergschrund above the TZ (Fig. 7). While
348 velocities were measured over austral summer, we assume these average velocities are
349 maintained during the winter as the average annual temperature is near −20.7°C (Monaghan et
350 al., 2005) and ice thicknesses is < 75 m, suggesting the bed is likely frozen. The velocity
351 gradients result in tensile stresses towards the east and south, which match locations of observed
352 crevassing. The velocity measurements along the proposed road range from 0.29 m a^{-1} near
353 exposed bedrock towards the west, to 0.88 m a^{-1} closer to the eastern boundary of the grid (Fig.
354 7).

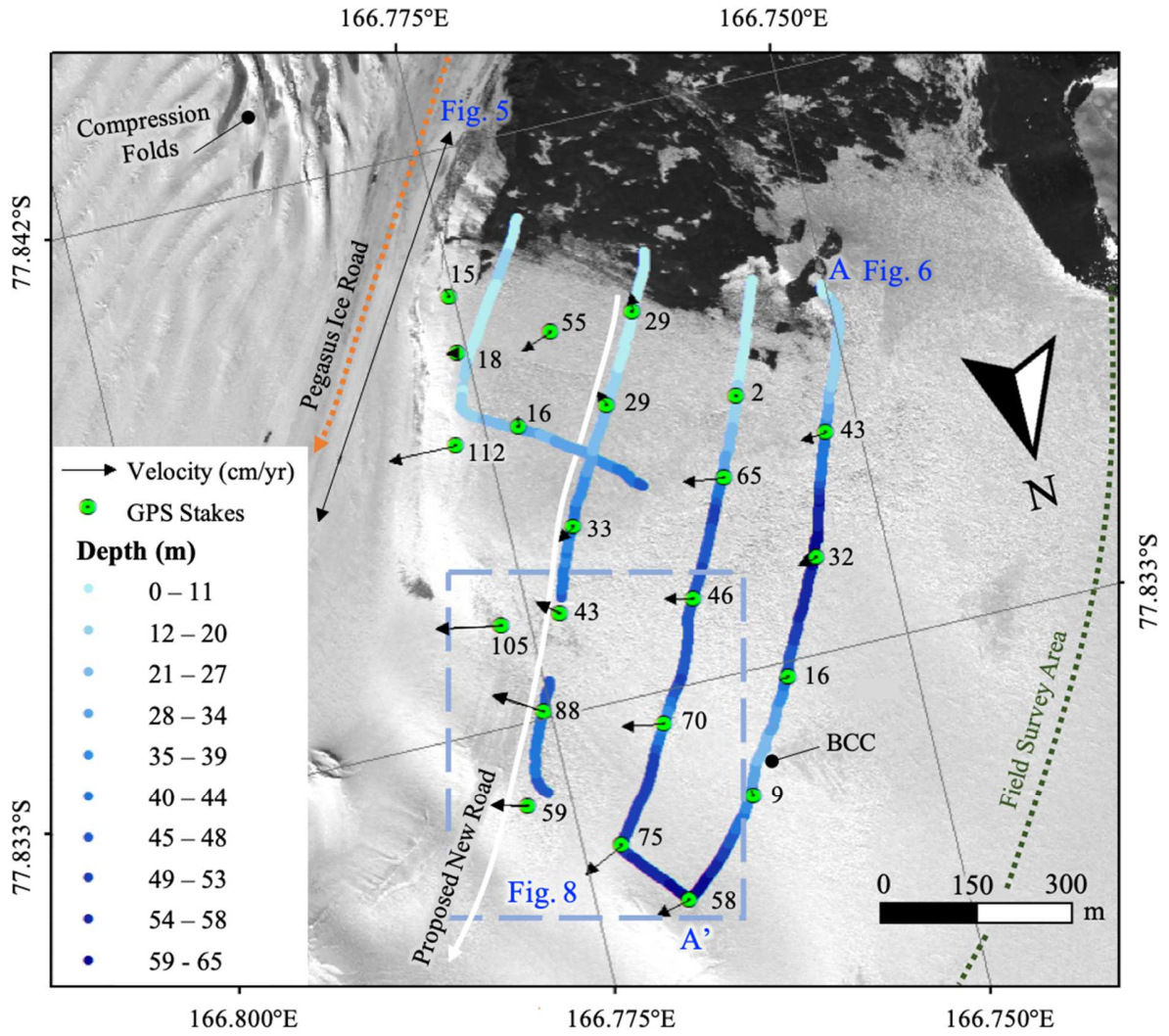

Figure 7. The Field survey area (inside green dotted line) of the TZ Hillside. Noted are the locations of the January 2016 GPR transects and the 2015-2016 repeat GPS survey stake locations (green circles). Transect colors indicate measured ice thicknesses and arrows indicate ice-flow velocities (magnitude and direction) measured by kinematic GPS surveys in November 2015 and January 2016. Also noted are the potential buried cinder cone (BCC), Pegasus Ice Road (orange dotted line), the approximate proposed road location (white solid line), and specific GPR transects shown in Figs. 5 and 6.

363

364 *3.3.2. Numerical modeling*

365 Three-dimensional numerical modeling was performed across the TZ Hillside,
366 specifically focusing on ice velocities around the proposed new road location. Modeling results
367 show ice-flow velocities between 0.1 and 1.2 m a^{-1} across the TZ Hillside (Fig. 8), with an
368 average modeled ice velocity across the proposed road transect of 0.35 m a^{-1}. Velocities are
369 slowest near the western glacier margin where ice thicknesses approach 0 m depth, and over the
370 buried cinder cone (BCC) near the top of the TZ Hillside where velocities are on the order of 0.1
371 m a^{-1}. Model velocity result patterns align well with GPS-measured velocities (±0.1 m a^{-1}), but
372 are conservative in magnitude. We calculate the annual volume of ice crossing the road at the
373 proposed road slice (Fig. 8) and find that over 204 ±24 m^3 ($1.64 - 2.05 \times 10^5$ kg) of ice would
374 need to be quarried annually from ice flowing downhill to maintain a bare-earth (bedrock) road.

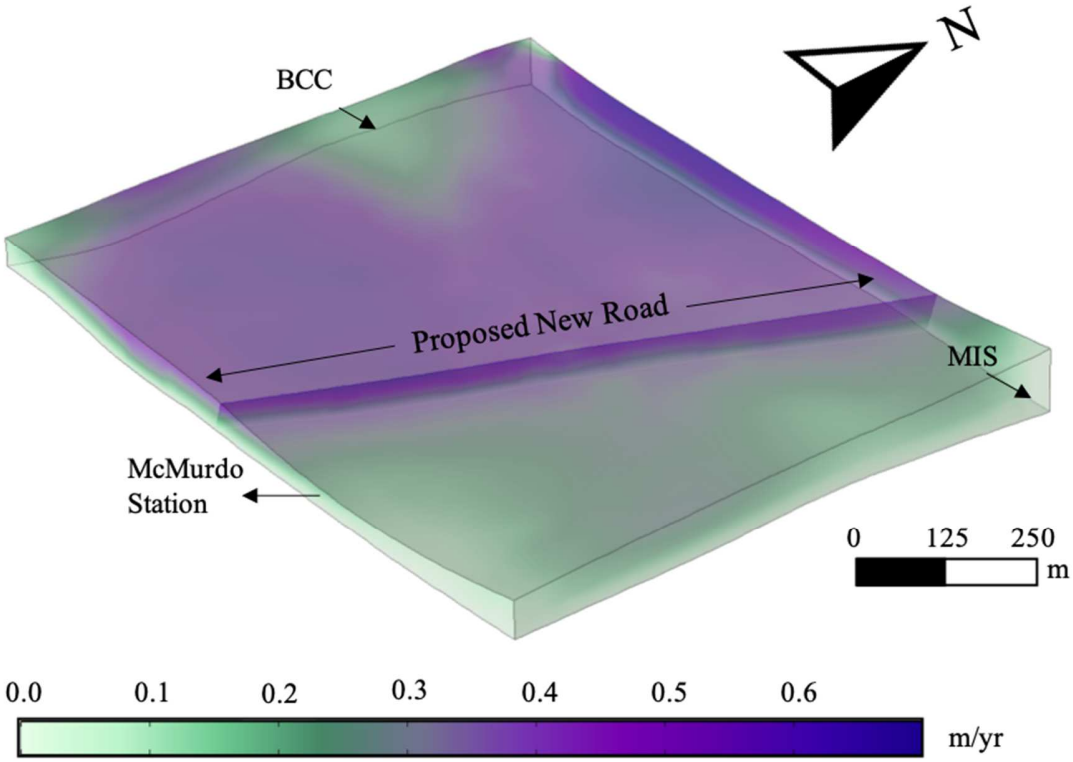

375

376 ***Figure 8. Temporal snapshot of the 3D TZ Hillside finite element numerical model showing***
377 ***modeled ice flow velocities (m a^{-1}) and a slice across the proposed new road. McMurdo***
378 ***Station is to the south and McMurdo Ice Shelf (MIS) and Grounding Line/Transition Zone***
379 ***(TZ) is to the east of the model. Model dimensions are based on GPR measured ice thickness***
380 ***and GPS measured elevation. Model velocities closely match observed velocities (±0.1 m a^{-1}),***
381 ***including low velocities over the potential buried cinder cone (BCC). The proposed road slice***
382 ***was used to integrate annual ice volume crossing the proposed road region.***

383

384 **4. DISCUSSION**

385 *4.1. McMurdo Ice Shelf Stability*

386 Differences in MIS elevation between 2011 and 2015 do not show any clear signal of
387 consistent elevation decrease, but instead show variable change across the study region. The
388 observed MIS terminus retreat between 2011 and 2015 was accompanied by an increase in
389 surface elevation near the terminus and a decrease farther upstream. We attribute the isolated
390 pockets of elevation change in the Pegasus Ice Road locations to be artificial (human-induced),
391 and from excavators quarrying snow to maintain the road or mitigate shifting snow drifts (Shoop
392 et al., 2014). The most dramatic change in ice elevation that was not artificially influenced,
393 occurs in the compression folds, aligning perpendicular to ice flow velocities (Fig. 4), indicating
394 that the pattern of alternating elevation gain and loss stems from shifting positions of peaks and
395 troughs of the compression folds. As this is a highly dynamic region, influenced by controlling
396 variables such as accumulation, ablation, and ice flow, movement of compression fold peaks
397 over an ~4-year period is a well-supported conclusion. The remainder of the flat MIS region
398 exhibits fairly uniform elevation loss or gain.
399 While the overall net change of the ice shelf is negative (-0.13 ± 1.11 m), the distribution
400 pattern of surface elevation change across MIS is positive near the terminus and negative
401 upstream; therefore, MIS terminus retreat currently appears to be more of a threat to MIS
402 stability than surface or basal melt. Previous GPR surveys across MIS revealed higher
403 accumulation rates near HPP on MIS than towards Black and White Islands (Campbell et al.,
404 2017). These high accumulation rates near HPP likely counter any summer surface or basal
405 melting, which suggests that the logistical use of MIS may safely continue as long as the MIS
406 terminus does not retreat to the TZ. However, MIS-HPP logistical concerns still exist, as
407 meltwater within the TZ is pooling at the firn-ice transition, which we expect to persist and
408 potentially increase, as melt on the TZ Hillside continues. Therefore, Pegasus Ice Road may

409 eventually need to be moved depending on future meltwater flux, thinning, and/or retreat of the
410 MIS terminus into the TZ.
411
412 *4.2. Hut Point Peninsula Stability*
413 While HPP is itself bedrock, Pegasus Ice Road connects MIS to both bases on HPP (Scott
414 Base and McMurdo Station), by way of crossing the TZ. The results presented here show that
415 the TZ Hillside currently has a negative mass balance, which could generate instability at the TZ
416 if or when the TZ Hillside decreases its ice mass contribution (influx) to the TZ. Therefore,
417 establishing potential alternative routes that removes the TZ crossing, is critical to uninterrupted
418 Antarctic science logistics. Surface elevation decreases on the northeast slope of HPP near the
419 TZ is prominent between 2011 and 2015, with an elevation loss between 1–2 m over the 4 year
420 study period. We interpret this surface lowering to be largely due to surface melt, with a lesser
421 component from sublimation, as strong Southerly winds were also reported during this study
422 period (Brett et al., 2020). We propose that this surface lowering is the primary source of
423 meltwater runoff pooling on the TZ, since the TZ Hillside is primarily composed of impermeable
424 ice (e.g., Shoop et al., 2014).
425 The GPR profiles and GPS surveys collected across the TZ Hillside evaluated a potential
426 alternative new road location. To install a road across the TZ Hillside, either blasting of ice to
427 place the road on solid ground, or grooming an ice road over the current surface, would need to
428 occur. Both options have major construction challenges, and each would require sizeable annual
429 maintenance. The TZ Hillside is predominantly ice, therefore minimal firn is readily available to
430 quarry for ice road maintenance. This does not account for the far greater volume of ice that
431 would need to be excavated to create an initial bare-earth (bedrock) road. The model results

suggest that a bedrock-based road would be more problematic to initially build and maintain, if not impossible, due to the sizeable volume of annual ice removal that would be required. However, the steep slope of the TZ Hillside would also make for potentially treacherous ice road conditions, due to meltwater drainage, refreezing, and snow drifts. These adverse conditions would need to be accounted for in design, building, and maintenance strategies prior to moving the current Pegasus Ice Road to the TZ Hillside.

4.3. DEM Differencing Caveats

Differencing corrected DEMs highlights elevation change in the region, however, some anomalies in the elevation data sets were not or could not be removed prior to differencing, primarily the movement of MIS and intra-seasonal variability. The DEMs from 2011 and 2015 were all acquired during austral summer, however intra-seasonal variability in storms and snow drifting could still contribute to some of the calculated elevation differences. These seasonal snow drifts are observable as isolated pockets of larger elevation change between bedrock outcrops on HPP. Steep slopes can also impact elevation calculations (e.g., Wang et al., 2019), which is especially true for large-scale features (10s m) within steep terrain. A majority of the terrain within this study maintains relatively consistent slopes across long distances (100s m); however, all slopes were considered over glaciated regions, and regions where slopes are >20° are isolated and therefore unlikely to have an impact on larger-scale changes (overall trends of net gains and losses). To date, there are no detailed studies of this region to quantifying the accumulation rate, therefore future investigations should include acquiring these data to enable the removal of small-scale seasonal impacts.

While we were able to resolve overall ice shelf elevation differences between 2011 and 2015, we were not able to resolve the nature of MIS thinning; specifically, if the elevation change resulted in a change of the ice shelf composition (percent of marine ice, glacier ice, accumulation), which is critical to ice shelf stability. Previous MIS studies suggest that marine ice reaches close to a third of the total MIS thickness (Arcone et al., 2016), but the distribution of marine ice under MIS (and most other ice shelves) is currently unknown. This is, in part, due to the difficulties of measuring ice shelf composition using GPR, as conductive attenuation prevents GPR from penetrating the full ice shelf thickness (e.g., Arcone et al., 2016), and also due to spatially sparse *in situ* measurements (i.e., borehole measurements; e.g., Craven et al., 2009). Other studies suggest significant annual thinning of MIS via basal melt, which would counter significant marine ice freeze-on (e.g., Rack et al., 2013; Stern et al., 2013; Tinto et al., 2019). This discrepancy between freeze-on and melt, and a lack of marine ice thickness observations, is perhaps one of the greatest unknowns to MIS stability. To better resolve ice shelf stability, future marine ice thickness measurements are critical to better contextualize changes in ice shelf elevation.

5. CONCLUSIONS

The MIS-HPP region serves as the primary logistics hub for both the United States and New Zealand Antarctic Programs. The MIS also buttresses several tributary glaciers and is critical to the stability of the Ross Ice Shelf. Problematically, MIS is disproportionately susceptible to potential disintegration, due to high surface and basal melt rates, meltwater pooling, and tidal flexure. If MIS were to weaken or collapse, the United States and New Zealand Antarctic science programs would also incur sizeable logistics challenges. Here we

focused on measuring the changes in ice elevation across MIS and HPP, and assessing a potential new access road between MIS and HPP. Through differencing DEMs collected in the austral summers of 2011 and 2015, we identified regions of large elevation change (~ ± 2 m), as well as MIS terminus retreat. The GPR surveys along Pegasus Ice Road found that the TZ crossing maintains pooled meltwater at the firn-ice transition, which can weaken the ice in this triaxial confluence of the HPP, MIS, and McMurdo sea ice. Additionally, GPR and GPS surveys on the TZ Hillside, as well as a resulting numerical model, explored the possibility of relocating the Pegasus Ice Road to bypass the TZ crossing. Results from the GPR, GPS, and numerical model showed that installation of a bare-earth (bedrock) road or ice surface road would require either sizeable glacier ice excavation or complex engineering on steep glacier terrain to bypass the current TZ crossing. Both scenarios would also require nearly constant maintenance due to glacier ice creep, melt, and snow drifting. While changes in ice elevation across the MIS-HPP region indicate no immediate need for rerouting Pegasus Ice Road to avoid the TZ crossing, GPS, GPR and modeling results also did not suggest a straightforward immediate rerouting solution. However, due to increasing ocean and atmospheric temperatures, combined with the vulnerability and importance of MIS to Antarctic logistics, continued remote sensing and *in situ* monitoring of this region is essential to exploring alternative MIS-HPP access points. Additionally, MIS is intrinsically connected to both East and West Antarctica through its shared boundary with the Ross Ice Shelf, such that changes in MIS will extend beyond the MIS region. These teleconnections necessitate that changes in MIS elevation, velocity, and ice thickness (including basal marine ice thickness) be quantified and monitored more extensively across this region to capture potential dynamical changes, which could prelude additional, far-reaching, dynamic responses.

ACKNOWLEDGEMENTS

Financial support for fieldwork was provided by NSF-OPP to EPOLAR (at CRREL) award number EP-ANT-16-32, and the surface elevation data were supplied by the Byrd Polar, Climate Research Center, and the Polar Geospatial Center under NSF-OPP awards 1543501, 1810976, 1542736, 1559691, 1043681, 1541332, 0753663, 1548562, 1238993 and NASA award NNX10AN61G. We thank UNAVCO for providing GPS support, and those that assisted with fieldwork data collection and processing, including Nate Lamie, John Fegyveresi, Chris Simmons, Jim Mediatore, Evan Miller, John Stone, Perry Spector, and Trevor Hillebrand.

DECLARATION OF INTERESTS

The authors declare that they have no known competing financial interests or personal relationships that could have appeared to influence the work reported in this paper.

REFERENCES

Arcone, S. A., Lever, J. H., Ray, L. E., Walker, B. S., Hamilton, G., & Kaluzienski, L. (2016), Ground-penetrating radar profiles of the McMurdo Shear Zone, Antarctica, acquired with an unmanned rover: Interpretation of crevasses, fractures, and folds within firn and marine iceGPR profiles of the McMurdo shear zone, *Geophysics*, 81(1), WA21-WA34.

Augustine, N. R., Allen, T., Dorman, C., Ducklow, H., Gordon, B., Harrison, R., & Wall, D. (2012), More and better science in Antarctica through increased logistical effectiveness, *Report of the US Antarctic Program Blue Ribbon Panel. Washington: White House Office of Science and Technology Policy and the National Science Foundation*.

Banwell, A. F., MacAyeal, D. R., & Sergienko, O. V. (2013), Breakup of the Larsen B Ice Shelf triggered by chain reaction drainage of supraglacial lakes, *Geophysical Research Letters*, 40(22), 5872-5876.

Banwell, A. F., Willis, I. C., Macdonald, G. J., Goodsell, B., & MacAyeal, D. R. (2019), Direct measurements of ice-shelf flexure caused by surface meltwater ponding and drainage, *Nature Communications*, 10(1), 1-10.

Bell, R. E., Chu, W., Kingslake, J., Das, I., Tedesco, M., Tinto, K. J., Zappa, C. J., Frezzotti, M., Boghosian, A., & Lee, W. S. (2017), Antarctic ice shelf potentially stabilized by export of meltwater in surface river, *Nature*, 544(7650), 344-348.

Brett, G., Irvin, A., Rack, W., Haas, C., Langhorne, P., & Leonard, G. (2020), Variability in the distribution of fast ice and the sub-ice platelet layer near McMurdo Ice Shelf, *Journal of Geophysical Research: Oceans*, 125(3), e2019JC015678.

Campbell, S., Kreutz, K., Osterberg, E., Arcone, S., Wake, C., Introne, D., Volkening, K., & Winski, D. (2012), Melt regimes, stratigraphy, flow dynamics and glaciochemistry of three glaciers in the Alaska Range, *Journal of Glaciology*, 58(207), 99-109.

Campbell, S., Courville, Z., Sinclair, S., & Wilner, J. (2017), Brine, englacial structure and basal properties near the terminus of McMurdo Ice Shelf, Antarctica, *Annals of Glaciology*, 58(74), 1-11.

Campbell, S., Lamie, N., & Schild, K. (2018), Structure and Stability of the McMurdo Ice Shelf Transition Zone and Glaciated Hillside near Scott Base, Antarctica, edited, ENGINEER RESEARCH AND DEVELOPMENT CENTER HANOVER NH HANOVER.

Child, S. F., Stearns, L. A., Girod, L., & Brecher, H. H. (2020), Structure-from-motion photogrammetry of Antarctic historical aerial photographs in conjunction with ground control derived from satellite data, *Remote Sensing*, 13(1), 21.

Craven, M., Allison, I., Fricker, H. A., & Warner, R. (2009), Properties of a marine ice layer under the Amery Ice Shelf, East Antarctica, *Journal of Glaciology*, 55(192), 717-728.

Depoorter, M. A., Bamber, J., Griggs, J., Lenaerts, J. T., Ligtenberg, S. R., van den Broeke, M. R., & Moholdt, G. (2013), Calving fluxes and basal melt rates of Antarctic ice shelves, *Nature*, 502(7469), 89-92.

Erofeeva, S., Padman, L., & Howard, S. (2020), Tide Model Driver (TMD) version 2.5, Toolbox for Matlab, edited, Github.

Fahnestock, M., Scambos, T., Moon, T., Gardner, A., Haran, T., & Klinger, M. (2016), Rapid large-area mapping of ice flow using Landsat 8, *Remote Sensing of Environment*, 185, 84-94.

Forster, R. R., Box, J. E., Van Den Broeke, M. R., Miège, C., Burgess, E. W., Van Angelen, J. H., Lenaerts, J. T., Koenig, L. S., Paden, J., & Lewis, C. (2014), Extensive liquid meltwater storage in firn within the Greenland ice sheet, *Nature Geoscience*, 7(2), 95-98.

Glasser, N., Goodsell, B., Copland, L., & Lawson, W. (2006), Debris characteristics and ice-shelf dynamics in the ablation region of the McMurdo Ice Shelf, Antarctica, *Journal of Glaciology*, 52(177), 223-234.

Haehnel, R. B., Blaisdell, G. L., Melendy, T., Shoop, S., & Courville, Z. (2019), A Snow Runway for Supporting Wheeled Aircraft: Phoenix Airfield, McMurdo, Antarctica, edited, ENGINEER RESEARCH AND DEVELOPMENT CENTER HANOVER NH HANOVER United States.

Hogg, A. E., Gilbert, L., Shepherd, A., Muir, A. S., & McMillan, M. (2021), Extending the record of Antarctic ice shelf thickness change, from 1992 to 2017, *Advances in Space Research*, 68(2), 724-731.

Howat, I. M., Porter, C., Smith, B. E., Noh, M.-J., & Morin, P. (2019), The reference elevation model of Antarctica, *The Cryosphere*, 13(2), 665-674.

Hulbe, C. L., Scambos, T. A., Youngberg, T., & Lamb, A. K. (2008), Patterns of glacier response to disintegration of the Larsen B ice shelf, Antarctic Peninsula, *Global and Planetary Change*, 63(1), 1-8.

Kingslake, J., Ely, J. C., Das, I., & Bell, R. E. (2017), Widespread movement of meltwater onto and across Antarctic ice shelves, *Nature*, 544(7650), 349-352.

Kulshrestha, A., Bahuguna, I., Rathore, B., & Iyer, K. V. (2020), Resolving Biases in DEM Differencing for Estimation of Change in Elevation of Glacier Surfaces Using Cartosat-I Stereo Data, *Journal of the Indian Society of Remote Sensing*, 48(10), 1443-1453.

Lever, J. H., & Thur, P. (2014), Economic analysis of the south pole traverse, edited, ENGINEER RESEARCH AND DEVELOPMENT CENTER HANOVER NH COLD REGIONS RESEARCH ….

583 MacGregor, J. A., Catania, G. A., Markowski, M. S., & Andrews, A. G. (2012), Widespread
584 rifting and retreat of ice-shelf margins in the eastern Amundsen Sea Embayment between
585 1972 and 2011, *Journal of Glaciology*, 58(209), 458-466.
586 Marshall, S. J. (2005), Recent advances in understanding ice sheet dynamics, *Earth and*
587 *Planetary Science Letters*, 240(2), 191-204.
588 McNabb, R. (2019), PyBob: A Python Package of Geospatial Tools, *Version 0.25*.
589 Millan, R. M., McCarthy, M. P., Sample, J. G., Smith, D. M., Thompson, L. D., McGaw, D. G.,
590 Woodger, L. A., Hewitt, J. G., Comess, M. D., Yando, K. B., Liang, A. X., Anderson, B.
591 A., Knezek, N. R., Rexroad, W. Z., Scheiman, J. M., Bowers, G. S., Halford, A. J.,
592 Collier, A. B., Clilverd, M. A., Lin, R. P., & Hudson, M. K. (2013), The Balloon Array
593 for RBSP Relativistic Electron Losses (BARREL), *Space Science Reviews*, 179(1-4),
594 503-530, doi:10.1007/s11214-013-9971-z.
595 Monaghan, A. J., Bromwich, D. H., Powers, J. G., & Manning, K. W. (2005), The climate of the
596 McMurdo, Antarctica, region as represented by one year of forecasts from the Antarctic
597 Mesoscale Prediction System, *Journal of Climate*, 18(8), 1174-1189.
598 Noh, M.-J., & Howat, I. M. (2015), Automated stereo-photogrammetric DEM generation at high
599 latitudes: Surface Extraction with TIN-based Search-space Minimization (SETSM)
600 validation and demonstration over glaciated regions, *GIScience & remote sensing*, 52(2),
601 198-217.
602 Nuth, C., & Kääb, A. (2011), Co-registration and bias corrections of satellite elevation data sets
603 for quantifying glacier thickness change, *The Cryosphere*, 5(1), 271-290, doi:10.5194/tc-
604 5-271-2011.
605 Padman, L., King, M., Goring, D., Corr, H., & Coleman, R. (2003), Ice-shelf elevation changes
606 due to atmospheric pressure variations, *Journal of Glaciology*, 49(167), 521-526.
607 Padman, L., & Erofeeva, S. (2005), Tide model driver (TMD) manual, *Earth and Space*
608 *research*.
609 Paul, F., Bolch, T., Kääb, A., Nagler, T., Nuth, C., Scharrer, K., Shepherd, A., Strozzi, T.,
610 Ticconi, F., & Bhambri, R. (2015), The glaciers climate change initiative: Methods for
611 creating glacier area, elevation change and velocity products, *Remote Sensing of*
612 *Environment*, 162, 408-426.
613 Paul, F., Bolch, T., Briggs, K., Kääb, A., McMillan, M., McNabb, R., Nagler, T., Nuth, C.,
614 Rastner, P., & Strozzi, T. (2017), Error sources and guidelines for quality assessment of
615 glacier area, elevation change, and velocity products derived from satellite data in the
616 Glaciers_cci project, *Remote Sensing of Environment*, 203, 256-275.
617 Rack, W., Haas, C., & Langhorne, P. J. (2013), Airborne thickness and freeboard measurements
618 over the McMurdo Ice Shelf, Antarctica, and implications for ice density, *Journal of*
619 *Geophysical Research: Oceans*, 118(11), 5899-5907.
620 Racoviteanu, A. E., Manley, W. F., Arnaud, Y., & Williams, M. W. (2007), Evaluating digital
621 elevation models for glaciologic applications: An example from Nevado Coropuna,
622 Peruvian Andes, *Global and Planetary Change*, 59(1-4), 110-125.
623 Reese, R., Gudmundsson, G. H., Levermann, A., & Winkelmann, R. (2018), The far reach of ice-
624 shelf thinning in Antarctica, *Nature Climate Change*, 8(1), 53-57.
625 Rignot, E., Jacobs, S., Mouginot, J., & Scheuchl, B. (2013), Ice-shelf melting around Antarctica,
626 *Science*, 341(6143), 266-270.

627 Scambos, T., Fahnestock, M., Moon, T., Gardner, A. S., & Klinger, M. (2019), Landsat 8 Ice
628 Speed of Antarctica (LISA), edited, NSIDC: National Snow and Ice Data Center,
629 doi:10.7265/nxpc-e997.
630 Scambos, T. A., Hulbe, C., Fahnestock, M., & Bohlander, J. (2000), The link between climate
631 warming and break-up of ice shelves in the Antarctic Peninsula, *Journal of Glaciology*,
632 46(154), 516-530.
633 Scambos, T. A., Bohlander, J., Shuman, C. A., & Skvarca, P. (2004), Glacier acceleration and
634 thinning after ice shelf collapse in the Larsen B embayment, Antarctica, *Geophysical*
635 *Research Letters*, 31(18).
636 Shoop, S. A., Hills, J., & Uberuaga, J. (2014), Maintenance and drainage guidance for the Scott
637 Base Transition, Antarctica.
638 Smith, B., Fricker, H. A., Gardner, A. S., Medley, B., Nilsson, J., Paolo, F. S., Holschuh, N.,
639 Adusumilli, S., Brunt, K., Csatho, B., Harbeck, K., Markus, T., Neumann, T., Siegfried,
640 M. R., & Zwally, H. J. (2020), Pervasive ice sheet mass loss reflects competing ocean
641 and atmosphere processes, *Science*, doi:10.1126/science.aaz5845.
642 Stern, A., Dinniman, M., Zagorodnov, V., Tyler, S., & Holland, D. (2013), Intrusion of warm
643 surface water beneath the McMurdo Ice Shelf, Antarctica, *Journal of Geophysical*
644 *Research: Oceans*, 118(12), 7036-7048.
645 Stewart, C. L., Christoffersen, P., Nicholls, K. W., Williams, M. J., & Dowdeswell, J. A. (2019),
646 Basal melting of Ross Ice Shelf from solar heat absorption in an ice-front polynya,
647 *Nature Geoscience*, 12(6), 435-440.
648 Tinto, K. J., Padman, L., Siddoway, C. S., Springer, S. R., Fricker, H. A., Das, I., Caratori
649 Tontini, F., Porter, D. F., Frearson, N. P., Howard, S. L., Siegfried, M. R., Mosbeux, C.,
650 Becker, M. K., Bertinato, C., Boghosian, A., Brady, N., Burton, B. L., Chu, W., Cordero,
651 S. I., Dhakal, T., Dong, L., Gustafson, C. D., Keeshin, S., Locke, C., Lockett, A.,
652 O'Brien, G., Spergel, J. J., Starke, S. E., Tankersley, M., Wearing, M. G., & Bell, R. E.
653 (2019), Ross Ice Shelf response to climate driven by the tectonic imprint on seafloor
654 bathymetry, *Nature Geoscience*, 12(6), 441-449, doi:10.1038/s41561-019-0370-2.
655 Wang, C., Zhu, X., Nie, S., Xi, X., Li, D., Zheng, W., & Chen, S. (2019), Ground elevation
656 accuracy verification of ICESat-2 data: A case study in Alaska, USA, *Optics express*,
657 27(26), 38168-38179.
658

659